Author Manuscript

Title: Deprotonation, Chloride Abstraction and Dehydrohalogenation as Synthetic Routes to bis-Pyrazolate Pyridyl Iron(II) Complexes

Authors: Brian J. Cook; Alexander V. Polezhaev, Ph.D; Chun-Hsing Chen, Ph.D.; Maren Pink, Ph.D.; Kenneth G. Caulton

This is the author manuscript accepted for publication and has undergone full peer review but has not been through the copyediting, typesetting, pagination and proofreading process, which may lead to differences between this version and the Version of Record.

To be cited as: 10.1002/ejic.201700558

Link to VoR: https://doi.org/10.1002/ejic.201700558

Deprotonation, Chloride Abstraction and Dehydrohalogenation as Synthetic Routes to bis-Pyrazolate Pyridyl Iron(II) Complexes.

Brian J. Cook,[a] Alexander V. Polezhaev,[a] Chun-Hsing Chen,[a] Maren Pink,[a] and Kenneth G. Caulton*[a]

The process of removal of protons and of chloride, dehydrohalogenation, from $(H_2L)FeCl_2$ is investigated systematically, to understand the reactivity of the implied transient LFe^{II}. Reaction of $(H_2L)FeCl_2$ with 2 equivalents of $LiN(SiMe_3)_2$ yields the "-ate" complex $LiClFe_2L_2$, as its dimer with every iron 5-coordinate in an FeN_4Cl environment. To avoid Li^+ cation derived from $LiN(SiMe_3)_2$, reaction of Na_2L with $FeCl_2$ gives a product from *addition* of water, paramagnetic $Na_2[NaFe(HL)(L)]_2(LFeO)$, which reveals Na/pyrazolate Nβ interactions and a five coordinate oxo group in the OFe_3Na_2 core of this aggregate. Abstraction of chloride in $(H_2L)FeCl_2$ with $NaBArF_4$ in THF gives paramagnetic $(H_2L)Fe(THF)_3^{2+}$ which fails to react with CO. Dehydrohalogenation in the presence of $Ph_2PC_2H_4PPh_2$, dppe, gives both $[LFe(\kappa^2\text{-dppe})]_2(\mu\text{-dppe})$ and $LFe(\kappa^2\text{-dppe})(\kappa^1\text{-dppe})$, diamagnetic saturated species which can be separated by pentane extraction. Dehydrohalogenation in the presence of ^{t}BuNC gives diamagnetic $LFe(CN^tBu)_3$. This is selectively methylated at both pyrazolate β-nitrogens to give $L^{Me}Fe(^tBuNC)_3^{2+}$ which shows rich cyclic voltammetry, and which is reduced, with KC_8, to diamagnetic $L^{Me}Fe(^tBuNC)_2$. Structure determination of certain of these, together with IR data on isonitrile stretching frequencies, show L^{2-} to be a stronger donor than L^{Me}. First installing triflate (to avoid the more persistent chloride ligand) facilitates access to $LFe(Lewis\ base)_3^{2+}$ complexes, but this cation still shows relatively weak binding of CO to LFe^{II}, which implicates weak π basicity of that d^6 species. Production of paramagnetic *bis*-pincer complexes $(H_2L)_2Fe^{2+}$ and $(L^{Me})_2Fe^{2+}$ in the presence of abundant Lewis base in polar medium is demonstrated, which illustrates a pincer ligand *redistribution* challenge to be kept in mind when trying to maintain a 1:1 Fe:pincer ratio, for highest reactivity.

Introduction

The connectivity choice between pyridine ortho positions and pyrazole ring positions has great impact on the communication between these two functionalities.[1] Connection (Fig. 1) using a pyrazole nitrogen (**A**) fixes this atom as sp^3 hybridized and thus interrupts the inter-ring conjugation in a way which *remains* (**B**) when a pyrazole carbon is the juncture.[2] The C-C connection in **B** also leaves the second pyrazole nitrogen an active (weakly acidic) functionality for later deprotonation[1c] or for hydrogen bonding.[1d, 1e, 3] The pyrazole β-nitrogen in **B**, when deprotonated, becomes a strong nucleophilic donor which can coordinate different metal electrophiles, or can be alkylated to shut down proton responsivity.[4] The former connection **A** diminishes the potential redox activity[5], while the 1,4 diazabutadiene character in **B** (highlighted in red) makes it a pyridine diimine (PDI) analog[6], but with an election donating *substituent* on one redox active nitrogen[7]; this electronic communication is also distinct from the typical aryl PDI substituent, where the aryl plane is orthogonal to the imine π system, and thus isolated. Finally, the pyrazole in **A** is an electron donating group to pyridine, but pyrazole in **B** is an electron withdrawing substituent on pyridine.

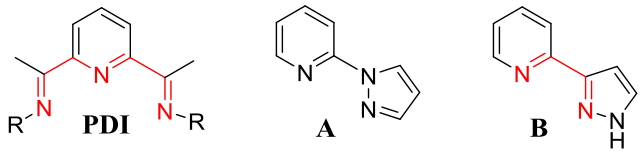

Figure 1. PDI ligand and two types of pyrazole-to-pyridine junction.

Our goal is to synthesize pincer H_2L (H_2L = 2,6-bis(5-(*tert*-butyl)-1H-pyrazol-3-yl)pyridine) ligated species of *unsaturated* divalent iron, thus ones of formula $LFe(Lewis\ base)_2$, and this demands synthetic access to the moiety LFe. We applied dehydrochlorination strategy (a redox-neutral process when hydrogen is removed from a ligand and chloride from iron by reacting with base) to achieve this goal and di- and triiron "aggregates" were isolated and characterized. Different Lewis bases were explored to break those "aggregates" apart and coordinate with species "LFe". However, those Lewis bases should be labile, to access an "LFe" fragment for substrate binding. Another question is the impact of spin state of the anticipated mononuclear iron complexes; does a spin state change make a reaction kinetically sluggish, and does a spin change impose a thermodynamic penalty on the conversion?[8] We therefore undertook a fundamental and wide-ranging series of studies to evaluate what nucleophiles can break the aggregate and the characteristics of the resulting products. As a preliminary study, we were interested in removing H^+ and Cl^- from $(H_2L)FeCl_2$ in a *stepwise* fashion, to avoid retention of LiCl in the final product, to target monomeric 1:1 LFe^{II} complexes. Our attempts towards $LFe(Lewis\ base)_2$ are summarized in Scheme 1.

[a] Brian J. Cook, Dr. Alexander V. Polezhaev, Dr. Chun-Hsing Chen, Dr. Maren Pink, and Prof. Dr. Kenneth G. Caulton
Department of Chemistry, Indiana University,
800 East Kirkwood Avenue, Bloomington, Indiana 47405, USA
Fax: +1-812-855-0985
E-mail: caulton@indiana.edu

[Supporting information for this article is given via a link at the end of the document.((Please delete this text if not appropriate))

Author Manuscript

This article is protected by copyright. All rights reserved

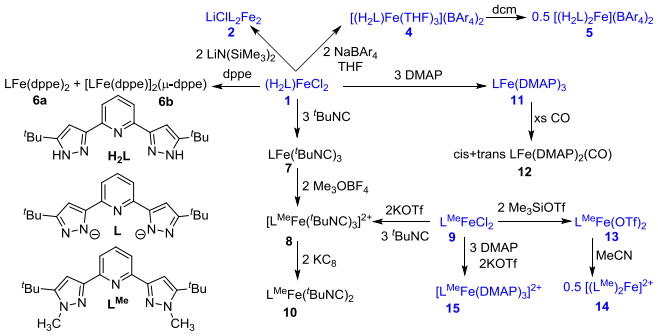

Scheme 1. Synthetic routes employed. Paramagnetic compounds labeled blue and diamagnetic are black; dppe = 1,2-bis(diphenylphosphino)ethane, DMAP = 4-dimethylaminopyridine.

Results and Discussion

Dehydrochlorination of $(H_2L)FeCl_2$

Dehydrohalogenation, the removal of a ligand-based proton and a halide from a metal (Scheme 2) can be an effective tool for opening metal coordination sites for substrate binding. Here, the proton-responsive pyrazole can be an effective Bronsted acid in dehydrohalogenation, yielding pyrazolate, which creates an amide (bound to the metal) and unmasks an outwardly directed β-nitrogen lone pair. Pincer ligands containing pyrazole have been shown to be competent for dehydrohalogenation, and this process is reversible on Ru.[1c] The choice of base can be critical in this reaction, and $LiN(SiMe_3)_2$ is attractive because its conjugate acid is bulky and volatile, so its subsequent binding to the (unsaturated) metal in LFe (Scheme 2) is discouraged, and it is readily removed in vacuo.

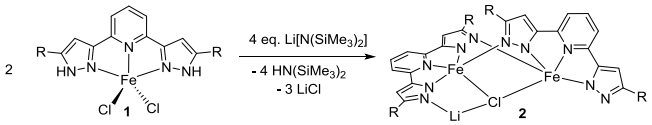

Scheme 2. Dehydrochlorination of compound **1** $(H_2L)FeCl_2$ with formation of Cl-bridged dimer **2**.

Dehydrohalogenation of $(H_2L)FeCl_2$ (**1**) with $LiN(SiMe_3)_2$ (1:2 mole ratio) in THF proceeds smoothly to yield a product whose proton NMR spectrum in d_8-THF shows full removal of NH protons and is a paramagnetic product with chemical shifts (+90 to – 20 ppm) and intensities indicating inequivalent arms in the pincer ligand: a total of five chemical shifts for ring protons, and two ^{t}Bu chemical shifts (S6). Single crystal X-ray diffraction of crystals grown from non-coordinating benzene/pentane solvent pair yields (Figure 2) a formula $[LiClFe_2L_2]_2$•2THF (**2**). Solvent molecule (THF) is retained even when recrystallized from benzene solvent. Each half of this dimer (Figure S3) contains the $Fe_2L_2Cl^-$ unit of Scheme 2. Each iron has a five coordinate trigonal pyramidal environment[9], and pairs of Fe are linked by two pyrazolate bridges and one chloride. The FeCl distances are in the narrow range 2.45 – 2.51 Å. The Fe-Fe distance, 3.27 Å, is well outside any bonding interaction but is ideal for the binding of chloride *between* the two Fe's. One Li^+ binds to both chlorides and to one pyrazolate nitrogen from each Fe_2L_2Cl unit, to achieve coordination number four. The other Li^+ binds to two THF and to one pyrazolate nitrogen, but not significantly to any chloride; this *three* coordinate and planar Li^+ is disordered (57:43 populations) into a second, symmetry-related site near nitrogen of the other $Fe_2L_2Cl^-$ unit (Figure S1). This Li^+ is the only thing that destroys what would otherwise be C_2 symmetry relationship of the two Fe_2L_2Cl units in this structure. Three of the four pyrazolate β nitrogens interact with some lithium. This structure is in accord with the observed ^{1}H NMR spectrum, but seeing only two ^{t}Bu chemical shifts means that Li2 migrates rapidly among two pyrazolates in any Fe_2L_2Cl unit. The structure is, operationally, a C_2 symmetric $LiClFe_2L_2$ unit.

The reason for dimerization of two $LiClFe_2L_2$ units is that one Li^+ binds two THF, and supplements those by one pyrazolate nitrogen while the other Li^+ binds no THF and thus links two Fe_2L_2 units by two chloride and two pyrazolate nitrogens. Any such L_2Fe_2 bimetallic fragment has 4-coordinate Fe(II), thus a high energy species, with a strong thermodynamic preference to bind a fifth ligand (here Cl^-) between the two Fe to make them 5-coordinate.

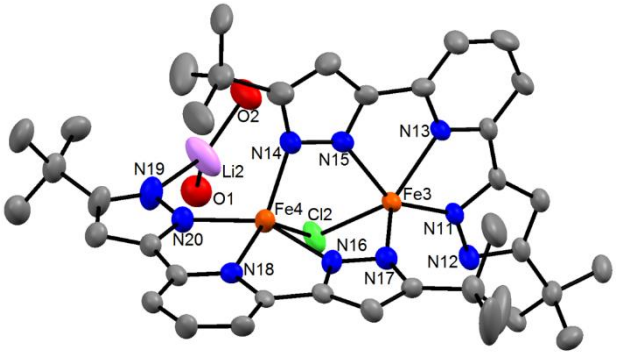

Figure 2. Mercury drawing (50% probability) of nonhydrogen atoms of $[LiClFe_2L_2]_2$ •2 THF showing only *half* of the dimer unit, hence $LiClFe_2L_2$. Cl2 and N12 bind to Li1 in second half of the dimer. The idealized C_2 axis goes through Cl2 and the Fe3Fe4 midpoint; the symmetry is broken by the $Li(THF)_2$ moiety, indicated by O1 and O2. Unlabeled atoms are carbons.

Deprotonation before Ligation: Retention of Alkali Metal Ion

An alternative strategy was to first deprotonate the *free* ligand, H_2L, with a strong base. Deprotonation of H_2L was achieved by adding excess (~5 molar excess) NaH to a THF solution of H_2L, which resulted in the immediate effervescence. Gas evolution completely ceased after 60 min, and the slurry was filtered through Celite to give a colorless solution (Scheme 3). This colorless solution was immediately added dropwise to a stirring slurry of $FeCl_2$ in THF (L:Fe = 1:1). This resulted in an immediate coloring of the solution to dark red, but eventually to a pale red, shown by ^{1}H NMR spectroscopy to contain a single product. Filtration, followed by removal of volatiles gave an orange-red solid which gave single crystals by slow diffusion of pentane

Author Manuscript

This article is protected by copyright. All rights reserved

vapors into a concentrated solution of product **3** in Et_2O. The ^1H NMR of this reddish solution gives a spectral pattern consistent with a polymetallic Fe^{II} species, consisting of 5 ^{t}Bu signals and 14 additional peaks, one of which has only half the intensity of the others (S9). This suggests *at least* a species featuring 5 pincer ligands, with ^{t}Bu groups pairwise-related by two-fold symmetry, and a unique pyridyl para-CH lying on the C_2 axis. Chemical shifts show a range of 45 ppm, establishing the product to be paramagnetic. This conclusion was further supported by single crystal X-ray diffraction.

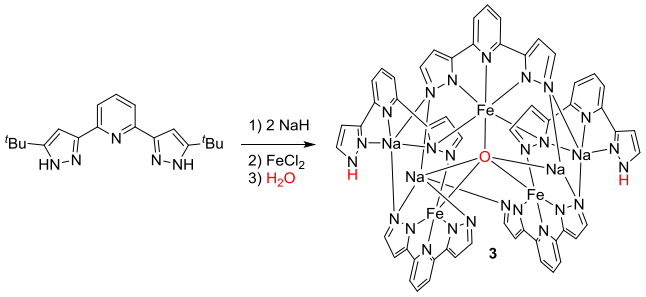

Scheme 3. Metallation of Na_2L with formation of tri-iron complex **3** (all ^{t}Bu groups are omitted for clarity).

Structural determination from these single crystals revealed a formula $H_2Na_4Fe_3L_5O$, better written as $Na_2[NaFe(HL)(L)]_2(LFeO)$ **3**. The structure (Figure 3) is consistent with the ^1H NMR data, and shows an aggregate with a total of 5 ligands, 3 Fe centers, and 4 Na^+. The structure has idealized (non-crystallographic) C_2 symmetry about the Fe2-N13 vector. There are two types of Fe implied by symmetry, Fe2 and Fe1/Fe3. The structure contains two symmetry related uncharged dimetal NaFeL(LH) units, where these two metals are held together by two bridging pyrazolates, one from each of two L. This resembles the $Fe_2L_2Cl^{-1}$ unit in compound **2**. These two units are linked by an Fe-O-Fe oxo bridge, and this oxo also binds to iron of the unique LFe2 unit, as well as to two Na^+ ions. The oxo is thus at the center of a trigonal bipyramidal Na_2Fe_3O unit; the oxide lies in the plane of the three irons. The two symmetry-related Fe are five coordinate. The unique iron, Fe2, augments its square planar surroundings by weak interactions with two pyrazolate nitrogens, at 2.424 and 2.673 Å. Each ligand L is planar except those two which donate to the unique iron, where the donor pyrazolate twists out of the plane of the pyridine. Every Na^+ interacts with pyrazolate nitrogens. The four Na atoms comprise two symmetry-related pairs. Two Na bind κ^3 to the pincer, with two additional interactions to neighboring pyrazolates. The other two, however, mix π and σ interactions with three neighboring pyrazolates, so each pyrazolate donating to Na is dihapto bound to two nitrogens. The only two pyrazolate nitrogens not donating to any metal, N1 and N21, carry the two protons in this molecule; those protons were found in final difference maps. One of these NH protons hydrogen bonds to a lattice Et_2O. The formidable product formula is dictated by Lewis acidity and charge balance: $[Fe_3Na_2(L^{2-})_5]^{2-}$ is balanced by Na_2O and 2 H^+. With this subdivision of the species, there are five planar ML_q units, which interact via bridging pyrazolates and the central μ_5 bridging oxide ion. This gives an overall synthetic stoichiometry of $2Na_2L + 3FeL + H_2O$. The product remains divalent Fe, but the L:Fe ratio is greater than 1:1.

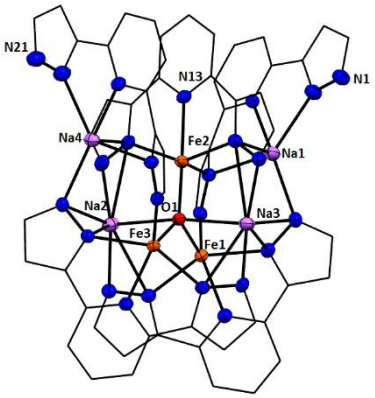

Figure 3. ORTEP representation (50%) of $Na_2[NaFe(HL)(L)]_2(LFeO)$ (**3**) showing selected atom labeling. Unlabeled atoms are nitrogen(blue). Hydrogens, ^{t}Bu-groups on pyrazoles and solvent guests removed for clarity; pincer core shown as wireframe.

Overall this structure shows the exceptional aggregating characteristics of the deprotonated bis-pyrazolate pincer, including its ability to incorporate alkali metal ions, when there are unused pyrazolate nitrogens β to the transition metal, and those alkali metals in turn incorporate small counter ions like O^{2-}. Even β–pyrazolate nitrogens not bound to Na^+ or Fe(II) find electrophiles (protons) to satisfy their Bronsted basicity; all pyrazolate nitrogens find a partner. The source of the oxygen cannot be inadvertent O_2, since all iron is unoxidized, as Fe^{II}. Therefore the oxide must originate from water[10] and/or Na_2O impurity in the NaH, due to the high oxophilicity of iron. Both oxophilic Fe and Bronsted basic L cooperate to deprotonate and bind H_2O. This highlights again the proton-responsive[4] character of this ligand, but binding Na^+ in multiple modes here also shows its *electrophile*-responsive character.

Chloride Removal from $(H_2L)FeCl_2$.

Considering chloride being responsible for aggregation of several "LFe" fragments and formation of compound **2** and metalation of Na_2L resulted in incomplete conversion we decided to first substitute chlorides in $(H_2L)FeCl_2$ **1** with non-coordinating counterion. Compound **1** reacts with $NaBAr_4$ ($BArF_4$ = (3,5-$(CF_3)_2C_6H_3)_4B$) (mole ratio 1:2) in THF to give $[(H_2L)Fe(THF)_3]^{2+}$ as a yellow microcrystalline solid (Scheme 4). The ^1H NMR of this species in CD_2Cl_2 reveals a signal pattern and δ range consistent with paramagnetic mononuclear Fe^{II} with C_2 symmetry (S11a). ^1H and ^{19}F NMR show signals corresponding to the aryl protons of $BArF_4$, as well as the CF_3 groups (-62 ppm), in a 2:1 $BArF_4$:L ratio (^1H NMR integration). The ESI-MS(+)mass spectrum in THF shows signals at 298.1 m/z, corresponding to $[(LH_2)Fe(THF)_3]^{2+}$ (**4**).

Author Manuscript

This article is protected by copyright. All rights reserved

Magnetic susceptibility measurement of this compound in CD_2Cl_2 at 25 °C using the Evans method gave a value of μ_{eff} of 4.48 μ_B, consistent with four unpaired electrons, hence S = 2. Single crystals suitable for X-ray diffraction, grown from diffusion of pentane vapor into a saturated THF solution, confirmed the formula to be $[(H_2L)Fe(THF)_3](BArF_4)_2$.

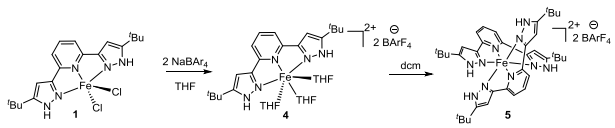

Scheme 4. Chloride abstraction from compound **1.**

The crystal quality prevented full refinement, but reveals connectivity (see Fig. S10) to show the success of the synthetic method. Attempts to recrystallized from dcm causes ligand redistribution and formation of homoleptic $(H_2L)_2Fe^{2+}$ (**5**) (that was characterized by X-ray diffractometry and proton NMR, see Fig. S9) and deprotonation attempts were unsuccessful and we decided to turn back to dehydrochlorination of **1** in presence of Lewis bases.

Isolation and Characterization of LFe(Lewis base)$_n$ Species

We were next interested in dissociation of the aggregate "-ate" complex $LiClFe_2L_2$ (**2**) to study the reactivity without the complication of multiple metal centers. Surprisingly, dehydrohalogenation of $(H_2L)FeCl_2$ in the presence of PEt_3 or CO failed to break apart the "-ate" complexes. Additionally, no reaction is observed when $LiClFe_2L_2$ is exposed to 1 atm of CO in C_6D_6 over the course of 24 h. Likewise, nitriles (PhCN, MeCN) fail to dissociate the aggregates. We therefore turned to other Lewis bases, and targeted unsaturated product LFe(base)$_2$, with either the bulky bidentate *bis*-diphenylphosphinoethane (dppe), the bulky isocyanide ^{t}BuNC and DMAP. A bidentate phosphine should be a stronger ligand than PEt_3 due to the chelate effect, and isocyanides are stronger σ-donors than nitriles.

Trapping with dppe, $Ph_2PCH_2CH_2PPh_2$.

Double deprotonation of $(H_2L)FeCl_2$ (**1)** with 2 moles of $LiN(SiMe_3)_2$ in Et_2O was followed by addition of dppe, $Ph_2PCH_2CH_2PPh_2$, at a Fe:chelate mole ratio 1.0:1.1, to form an orange-brown product over the course of 1 h (Scheme 5). Extraction into pentane separates two species formed in the reaction. One product is *diamagnetic*, as judged by ^{1}H and ^{31}P NMR experiments, and shows *four* $^{31}P(^1H)$ chemical shifts (S19a). This is clearly not the targeted unsaturated LFe(dppe). One of these chemical shifts is very similar to that of uncoordinated phosphine (free dppe at -11.7 ppm), but couples weakly to one other phosphorus atom; this last is assigned to a κ^1-dppe. The two furthest downfield doublet of doublets correspond to inequivalent phosphorus atoms in a second dppe ligand, and the final doublet of doublet of doublets is the coordinated phosphine of the κ^1-dppe. All J_{PP} coupling constants are in agreement with a formula LFe(κ^2-dppe)(κ^1-dppe) **6a**, of stereochemistry in Scheme 5. Also formed is a second *diamagnetic* product, with very similar chemical shifts and coupling constants, except for the absence of the pendant phosphine signal. This species then has *three* phosphorus signals with relative intensity 1:1:1, assigned as [LFe(κ^2-dppe)]$_2$(μ-dppe) **6b**.

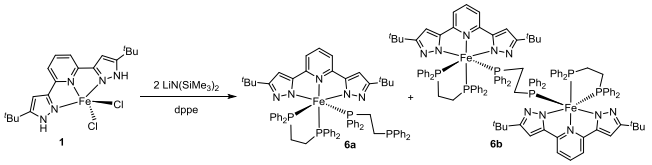

Scheme 5. Formation of LFe(κ^2-dppe)(κ^1-dppe) **6a** and LFe(κ^2-dppe)]$_2$(μ-dppe) **6b.**

These spectroscopic assignments were supported by ^{1}H NMR studies, including with ^{31}P decoupling (S20a-S21). Since both these products have higher P:Fe ratios than used in the synthesis, they indicate the lower thermodynamic stability of the desired 16 electron LFe(base)$_2$. Using 1.5 equivalents of dppe during dehydrohalogenation, in an attempt to favor formation of [LFe(κ^2-dppe)]$_2$(μ-dppe) **6b**, results in the same 1.0:0.6 product ratio observed from the original synthetic conditions. Employing 2.0 eq. of dppe yields only the product LFe(κ^2-dppe)(κ^1-dppe), which delivers the optimal yield for this synthesis at 92%. These two products are readily separated since LFe(κ^2-dppe)(κ^1-dppe) **6a** is soluble in pentane while [LFe(κ^2-dppe)]$_2$(μ-dppe) **6b** is negligibly so. The structural conclusions from NMR spectroscopy were supported by a single crystal structure determination of [LFe(κ^2-dppe)]$_2$(μ-dppe) **6b**. Crystals of [LFe(κ^2-dppe)]$_2$(μ-dppe) **6b** form from a pure sample of LFe(κ^2-dppe)(κ^1-dppe), so the two are thus in an equilibrium established over ~24 h at 25 °C, and [LFe(κ^2-dppe)]$_2$(μ-dppe) **6b** is favored in the solid state.

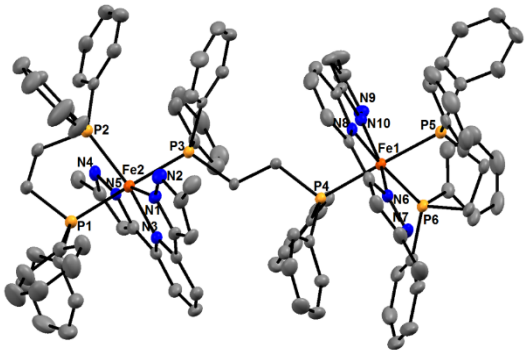

Figure 4. Mercury view of the nonhydrogen atoms of [LFe(dppe)]$_2$(dppe) **6b**, showing selected atom labeling. Unlabeled atoms are carbon; ^{t}Bu groups are omitted for clarity. Selected structural parameters (Å,°): Fe1-N8, 1.957; Fe1-N6, 2.005; Fe-N10, 1.992; Fe1-P5, 2.291; Fe-P6, 2.276; Fe1-P4, 2.329; N10-Fe1-N6, 157.14; P4-Fe1-P5, 178.48; P5-Fe1-P6, 82.82; N6-Fe1-N8, 78.88.

Author Manuscript

This article is protected by copyright. All rights reserved

Single crystal X-ray diffraction (Figure 4) reveals a structure for [LFe(κ^2-dppe)]$_2$(μ-dppe) **6b** in agreement with conclusions from spectroscopy, and allows some additional conclusions based on metrics. The three Fe/N distances are all shorter than those in the HS-Fe^{II} species characterized with this pincer, since the present compound is low spin, consistent with octahedral Fe^{II}. The Fe-N distances are shorter to pyridine than they are to pyrazolate. The three Fe/P distances are all different, shorter for the chelated dppe P donors, and longest for the bridging dppe. The conformation around the C-C bond in the bridging dppe is staggered, to minimize repulsions between the bulky octahedral complexes. The CNN angles within the pyrazolate rings are all 107 ±0.4^o, consistent with deprotonated pyrazolates[1c]

ESI-MS of a pure solid sample of LFe(κ^2-dppe)(κ^1-dppe) reveals only the ion LFe(dppe)$^+$, showing ready displacement of the pendant phosphine chelate (S22). Re-dissolving a crystalline sample of [LFe(κ^2-dppe)]$_2$(μ-dppe) shows by ^{31}P NMR a 5:1 ratio of LFe(κ^2-dppe)(κ^1-dppe) to [LFe(κ^2-dppe)]$_2$(μ-dppe), showing this equilibrium is rapidly established in solution, and that free dppe must co-crystallize with this species to maintain mass balance. Electrochemical study of compound **6b** was performed together with reactivity study toward oxidants (see S16-17b, S23).

Trapping with ^{t}BuNC

Analogous trapping of "LFe" during dehydrohalogenation was also attempted with ^{t}BuNC. Performing dehydrohalogenation (with LiN(SiMe$_3$)$_2$) of (H$_2$L)FeCl$_2$ (**1**) in the presence of ^{t}BuNC (Fe:^{t}BuNC mole ratio 1:2) in Et$_2$O gives rapid formation of a yellow-orange solution which, after removal of volatiles and extraction into pentane, yields a spectroscopically pure canary-yellow microcrystalline solid (Scheme 6).

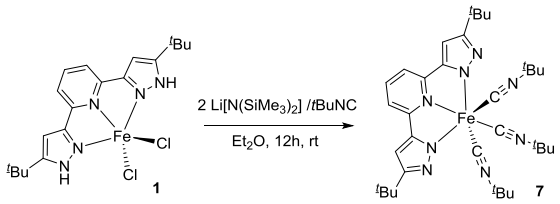

Scheme 6. Synthesis of LFe(^{t}BuNC)$_3$ **(7)**.

The ^{1}H NMR spectrum of this *diamagnetic* material in C$_6$D$_6$ is consistent with formula LFe(CN^{t}Bu)$_3$ (**7**) of C_{2v} symmetry (Scheme 6). Separate signals for the two types of ^{t}BuNC protons in a 2:1 ratio prove that any site exchange between these, or dissociation, is slow on the NMR time scale. Unsaturated LFe(CN^{t}Bu)$_2$ is not the product. The ^{13}C NMR spectrum corroborates this conclusion, as three peaks are observed in a 2:1:2 intensity pattern for the three types of ^{t}Bu protons (2 from ^{t}BuNC, 1 from the pincer). The FT-IR spectrum of this species in pentane shows three frequencies at 2157, 2131, and 2078 cm^{-1}, consistent with three C≡N stretches from ^{t}BuNC in a C_{2v} structure. Since the observed species contains more ^{t}BuNC than was supplied, a second product is implied. A benzene soluble fraction of the reaction solution shows NMR chemical shifts consistent with formula LiClFe$_2$L$_2$, devoid of ^{t}BuNC.

The mass spectrum of (**7**) (L)Fe(^{t}BuNC)$_3$ is informative of its reactivity. The ESI(+) mass spectrum in THF shows two sets of molecular cations. The first has m/z = 627.4, which corresponds to the protonated molecular cation [M+H]$^+$, better written as (LH)^{56}Fe(tBuNC)$_3^+$. This peak also has the corresponding ^{54}Fe isotopomer (6%) at 625.4 The second set of peaks is centered at 710.5, or 83.1 mass units greater than that of [M+H]$^+$, in agreement with the formula (LH)^{56}Fe(^{t}BuNC)$_4^+$ with the ^{54}Fe isotopomer apparent also. One possible explanation for the existence of this second cation is the dissociation of the pyrazole ring that has been protonated, and the coordination of a fourth isonitrile ligand. However, under APCI(+) ionization conditions, the [M+H]$^+$ peak at 627.5 is formed *exclusively*, without any intensity at 710.5. Formation of the tetrakis-isonitrile cation is favored under ESI(+) conditions only. In APCI(-) there is a peak centered at 698.3 which is consistent with the formula [M+THF]$^-$, with the ^{54}Fe isotopomer at 696.4, thus showing that this molecular anion contains Fe.

Structural characterization by single crystal X-ray diffraction (Figure 5) confirms the conclusions from spectroscopy and gives some useful metric parameters. Deprotonation at the pyrazolate β nitrogens is confirmed by the angle CNN (<106.5^o)[1c]. All Fe/N distances are short, consistent with LS-Fe^{II} LFe(CN^{t}Bu)$_3$. It is noteworthy that all three isonitriles are *bent* at nitrogen, 164.77(17)–160.90(16)^o, which indicates significant back donation, since π-donation effects a change in hybridization of nitrogen from sp to sp^2. However, it is has been conjectured in similar systems that this phenomenon is due to packing forces.[11]

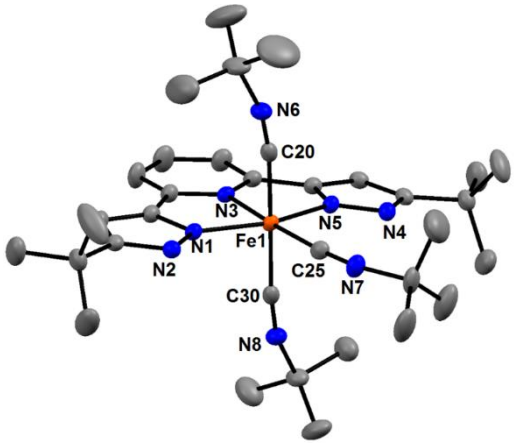

Figure 5. Mercury view of the nonhydrogen atoms of LFe(CN^{t}Bu)$_3$ (**7**), showing selected atom labeling. Unlabeled atoms are carbon. Selected structural parameters (Å): Fe1-C25, 1.8523(15); Fe1-C30, 1.8765(17); Fe1-C20, 1.8837(17); Fe1-N3, 1.9465(12); Fe1-N5, 1.9695(13); Fe1-N1, 1.9786(13).

Because LiClFe$_2$L$_2$ is inert to 1 atm of CO over the course of 24 h, this illustrates a subtle difference in these Lewis bases: CO is a weaker σ-donor than CNR, and thus is unable to dissociate the

Author Manuscript

This article is protected by copyright. All rights reserved

pyrazolate-bridged aggregates. Carbon monoxide is not a competent donor to LFe^{II}.

The cyclic voltammogram of $LFe(CN^tBu)_3$ shows (Figure 6) one reversible oxidation, showing retention of isonitrile ligands in newly formed $LFe(CN^tBu)_3^+$, and one *irreversible* reduction, near –2.5 V, consistent with reduction to Fe^I, but ready ligand loss in this 19 valence electron species; this was then tested with chemical reductant (see below).

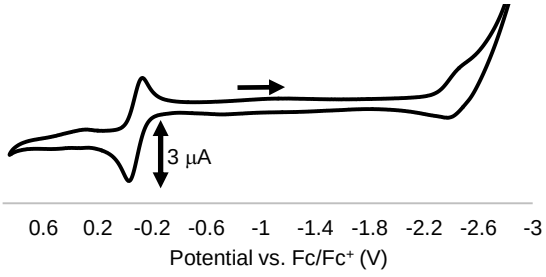

Figure 6: Cyclic Voltammogram for $LFe(^tBuNC)_3$. Arrow indicates scan direction and origin. Working Electrode: Pt. Auxiliary Electrode: Pt wire. Reference electrode: Ag wire. Referenced to internal Fc/Fc^+ couple. Scan rate: 50 mV/s. Supporting electrolyte: $[Bu_4N]PF_6$. Analyte Concentration: 1.6 mM.

Methylation of Coordinated Pincer Pyrazolate: Synthesis of $L^{Me}Fe(^tBuNC)_3^{2+}$

We tested the nucleophilicity of Nβ with an alkylating agent to allow insight into how this *bis*-pyrazolate pincer might interact with an even weaker electrophile, for example CO_2. Treatment of $LFe(^tBuNC)_3$ with 2 eq. Me_3OBF_4 in CH_2Cl_2 results in a color change over the course of 1 h from yellow to orange. The reaction is initially heterogeneous (insoluble Me_3OBF_4), but becomes homogeneous as the reaction goes to completion. The doubly alkylated product, $[L^{Me}Fe(^tBuNC)_3](BF_4)_2$, was obtained in 93% yield and was characterized by ^1H, ^{13}C, and ^{19}F NMR spectroscopy, as well as FT-IR, mass spectrometry and single crystal X-ray diffraction (Scheme 7).

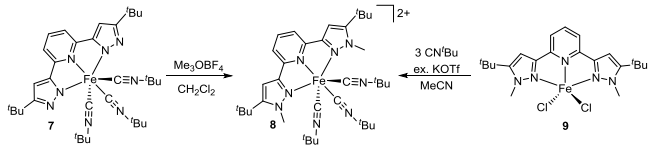

Scheme 7. Probing nucleophilicity of pyrazolate β-nitrogens.

The ^1H NMR spectrum of this *diamagnetic* species in CD_2Cl_2 shows a downfield shift of all peaks compared to $LFe(CN^tBu)_3$ (**7**). The biggest difference in the spectrum is the appearance of a peak at 3.86 ppm, which corresponds to the equivalent N-Me peaks of the newly doubly alkylated two-fold symmetric pyrazole rings. The signal integral ratio of 18:18:9 for the ^{t}Bu peaks indicates retention of all three isonitrile ligands upon double alkylation. The FT-IR spectrum confirms less π-back-bonding in the dication, as all three υ_{CN} peaks shift to higher energy (2205, 2178, 2164 cm^{-1}). The ESI(+) mass spectrum of this species in THF solvent confirms its identity and successful double alkylation with a strong signal at m/z = 743.3, which corresponds to the ion pair $[L^{Me}Fe(^tBuNC)_3](BF_4)^+$ (**8**), together with all expected isotopologs for those nuclei. Collectively, the spectroscopy confirms selective pincer *bis*-alkylation regiochemistry via this template synthesis methodology, with no alkylation at any other site in the molecule.

Single crystals were obtained from CH_2Cl_2 and reveal (Figure 7) a similar geometry around Fe^{II} as in the starting material, with two new C-N bonds on the pyrazole ring, confirming the alkylation regiochemistry. Each of the isonitrile ligands are now more linear compared to the neutral complex (C-N-C(^{t}Bu) = 175° vs. 160°), which is in good agreement with the conclusion from FT-IR of less back donation to the ^{t}BuNC ligands in the dication. Accordingly, Fe/C distances are longer by ~0.02 Å in the dication and Fe/N(pyrazolate) are longer by ~0.03 Å. The alkylated pyrazole L^{Me} is a weaker donor than the anionic pyrazolate L^{2-}, but the dication is still low spin Fe^{II}. Since the bond length changes are quite small, the overall effect is better realized in the FT-IR measurement.

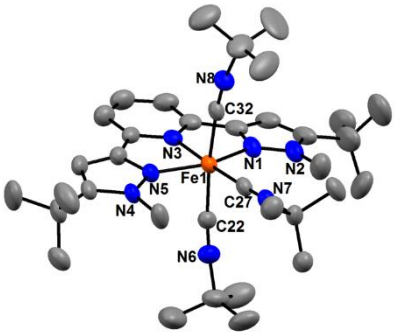

Figure 7. Mercury representation of the nonhydrogen atom of the dication (**8**) in $[L^{Me}Fe(^tBuNC)_3](BF_4)_2$, showing selected atom labelling; unlabeled atoms are carbon. Selected structural parameters: Fe1-C27, 1.875(5) Å; Fe1-C32, 1.909(5); Fe1-C22, 1.911(5); Fe1-N3, 1.949(4); Fe1-N1, 2.011(4); Fe1-N5, 2.017(4); C22-N6-C23, 175.0(6)°; C27-N7-C28, 178.7(5); C32-N8-C33, 169.1(5).

The $[L^{Me}Fe(^tBuNC)_3]$ dication was synthesized using an alternative approach. Reaction of of $L^{Me}FeCl_2$ in MeCN with excess KOTf the presence of 3 equivalents of tBuNC at room temperature (Scheme 7) leads to a dark orange solution within 10 min of mixing, ^1H NMR spectra of the isolated product shows diamagnetism and the same signals for $L^{Me}Fe(^tBuNC)_3(BF_4)_2$ obtained by methylation of $LFe(^tBuNC)_3$. ^{19}F NMR confirms the presence of TfO^-.

Reductive conversion to $L^{Me}Fe(^tBuNC)_2$ 10

We expected the charge of the doubly alkylated product, $[L^{Me}Fe(^tBuNC)_3](BF_4)_2$, to facilitate its reduction. The goal was to have *coordinated* ^{t}BuNC serve as an *in situ* trap for Fe^0, avoiding the inefficiency of adding additional trapping agent after reduction. The alkylated species is insoluble in benzene, but reduction of a benzene suspension of this dication with 2 eq. of

Author Manuscript

This article is protected by copyright. All rights reserved

KC_8 results in an immediate color change to yellow (Scheme 8). This reaction is reproducible in toluene solvent. Removal of graphite by filtration reveals a dark yellow-orange filtrate. The increased solubility is consistent with conversion to a neutral species, however the product is poorly soluble in linear alkanes.

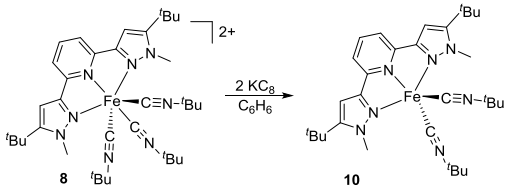

Scheme 8. Reduction of dicationic complex **8**.

The ^{1}H NMR spectrum of the reduction product shows sharp peaks in the range 0-10 ppm, consistent with *diamagnetism*; signals of the starting material are completely consumed. Additionally, the new diamagnetic product shows two-fold symmetry of the pincer ligand. Two peaks each integrate for 18 protons, showing two equivalent pincer ^{t}Bu groups and those derived from *two* isonitrile ligands (S29). Overall, the NMR spectroscopy supports a diamagnetic 2-electron reduction product of formula $L^{Me}Fe(^tBuNC)_2$ (**10**), with equivalent isonitrile ligands. FT-IR spectroscopy (S25) also supports this formula, with 2 ν_{CN} stretches that have shifted to lower energy (2145, 2076 cm^{-1}) *vs.* the dication, consistent with a loss of an isonitrile ligand and a higher degree of π-back-bonding from a lower valent Fe center.

A Weaker Lewis Base: LFe(DMAP)$_3$

We employed *para* dimethylamino pyridine, DMAP, seeking a five-coordinated LFe(DMAP)$_2$, or a *high spin* six-coordinate species, and faster rates of reaction with CO due to population of σ_{ML}* orbitals in octahedral d^6 species. Dehydrohalogenating $(H_2L)FeCl_2$ in the presence of *two* equivalents of DMAP (DMAP = 4-dimethylaminopyridine) with 2 equivalents of $LiN(SiMe_3)_2$ in toluene at room temperature leads to a dark red solution within 10 min of mixing (Scheme 9).

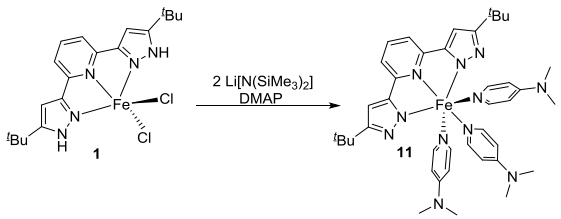

Scheme 9. Formation of *tris*-DMAP adduct **11**.

Filtration and removal of volatiles yields a mesa-red powder which is soluble in most common laboratory solvents except for alkanes. The ^{1}H NMR spectrum of this species in C_6D_6 reveals the molecule to be *paramagnetic*, with a proton chemical shift range of +50 to -10 ppm. One peak at 4.53 ppm is assigned to ^{t}Bu ligand based on its relative intensity, however there also exist peaks corresponding to 12H and to 6H, which suggest *three* DMAP ligands in a *mer* geometry. Loss of NMe_2H to give a cation observed by ESI mass spectrometry is suggested to involve protonation of DMAP nitrogen, then amine elimination. Duplicate Evans method magnetic susceptibility determinations at 25 ºC reveal spin-only μ_{eff} values of 4.5 and 4.6 μ_B, which correspond to 4 unpaired electrons, or high spin Fe^{II}, S = 2. Magnetometric studies of LFe(DMAP)$_3$ **11** shows it to exhibit temperature dependent spin-crossover behavior[12] (see S32a-33).

Single crystal X-ray diffraction structure determination led to the structure shown in Figure 8. The asymmetric unit contains two molecules, but these show no significant differences so the discussion will employ the molecule illustrated. A least squares fit of the two independent molecules shows that even the rotational conformation of the DMAP planes is analogous (see S28). This confirms a wholly planar pincer ligand with a *mer*-arrangement of three DMAP donors, yielding a six-coordinate arrangement of donors around Fe. The pincer pyridine forms FeN bonds 0.03 - 0.07 Å shorter to iron that to the pyrazolates, and there are no clear inequivalencies in Fe-N(DMAP) distances for those trans to pincer pyridine *vs.* trans to another DMAP.

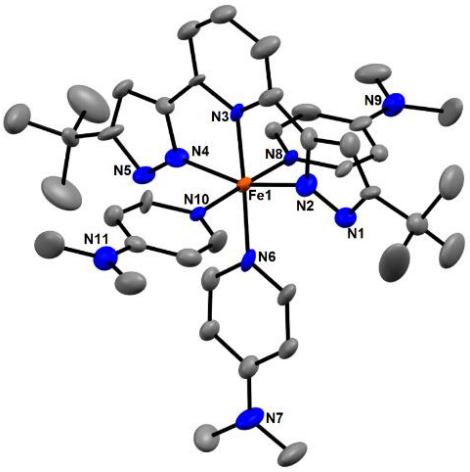

Figure 8. Mercury view of the nonhydrogen atoms of (L)Fe(DMAP)$_3$ **11** at 150 K, showing selected atom labeling. Unlabeled atoms are carbon. Selected structural parameters (Å); data for second molecule shown in parentheses: Fe1-N2, 1.999(6)(1.992(7)); Fe1-N3, 1.967(7)(1.939(7)); Fe1-N4, 2.086(7)(2.066(7)); Fe1-N6, 2.047(7)(2.017(7)); Fe1-N8, 2.063(6)(2.045(7)); Fe1-N10, 2.072(6)(2.072(7)).

Ligand Substitution Chemistry on LFe(DMAP)$_3$: Synthesis of LFe(DMAP)$_2$(CO)

We were interested in the substitution *lability* of paramagnetic LFe(DMAP)$_3$ towards a probe ligand which at the same time delivers a useful spectroscopic parameter, CO. We were also interested in the number of CO which this complex would add, and also the spin state of the resulting product. Reaction of LFe(DMAP)$_3$ with equimolar CO in CD_2Cl_2 occurs (Scheme 10)

Author Manuscript

This article is protected by copyright. All rights reserved

in time of mixing with color change from deep-red to yellow and shows ^{1}H NMR signals of free DMAP and another *diamagnetic* product containing signals from both L and DMAP. The same reaction performed in toluene-d_8 occurs with rapid bleaching of color with complete conversion. This solution quickly deposits red solid which, following filtration and washing with pentane to remove any free DMAP, shows proton NMR in CD_2Cl_2 consistent with that synthesized in toluene.

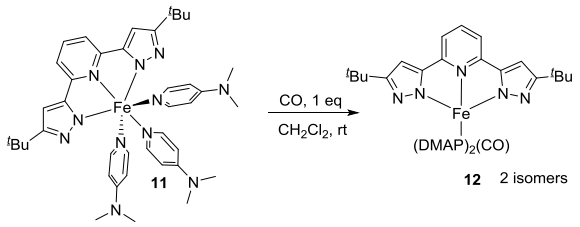

Scheme 10. Reaction of LFe(DMAP)$_3$ (**11**) with CO.

Single crystals grown by slow diffusion of pentane into a saturated solution in dichloromethane show (Figure 9) formula LFe(DMAP)$_2$(CO) as an octahedral structure with the two DMAP ligands mutually *trans*. Both NNC angles around the pyrazole β nitrogen are 106°[1c], confirming that the pincer ligand here carries no protons. This is further supported by the observation that a guest molecule of CH_2Cl_2 forms a hydrogen bond from its H to one pyrazolate β nitrogen (see S34). Other features of this structure are unexceptional, and the DMAP ring nitrogens, in spite of the planar NMe_2 substituents (electron donating), form longer bonds to iron than does any nitrogen of the pincer as in the previous LFe(DMAP)$_3$ structure. The Fe/N distances in LFe(DMAP)$_2$(CO) are consistently shorter (by 0.04 – 0.06 Å) than to those of LFe(DMAP)$_3$ at -150 °C (at which temperature it is partly in the low-spin state), a difference we attribute to the carbonyl complex being purely S = 0. This spin state change reflects the expectation that CO is a strong field ligand compared to any pyridine, even DMAP.

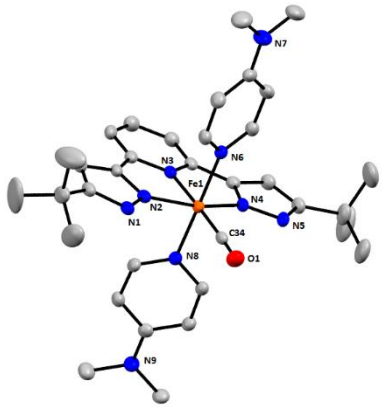

Figure 9. Mercury drawing of the nonhydrogen atoms of LFe(DMAP)$_2$(CO) **12**, showing selected atom labelling; unlabeled atoms are carbon. Selected structural parameters: Fe1-N2, 1.9476(18) Å; Fe1-N3, 1.943(2); Fe1-N4, 1.9575(17); Fe1-N6, 2.0402(18); Fe1-N8, 2.0125(18); Fe1-C34, 1.773(3); O1-C34, 1.148(3); O1-C34-Fe1, 177.20(19); N3-Fe1-N6, 88.38(7); N3-Fe1-N8, 88.85(7); N3-Fe1-C34, 177.59(9).

Proton NMR of pure samples of isolated mixture of cis/trans LFe(DMAP)$_2$(CO) were examined both in dichloromethane and in toluene-D_8 solvent (see Supporting Information). Together these results show signals consistent with two isomers, those with DMAP both *trans* and *cis in ~0.8:1 cis/trans ratio*. These mixtures show two ^{t}Bu signals and two pyrazolate signals and two *para*- and two *meta*-pincer pyridine signals with appropriate multiplicity. One NMe_2 signal is seen for the *trans* isomer and two are resolved in dichloromethane for the *cis* isomer. Finally, the spectra show two chemical shifts for DMAP ring protons in the *trans* isomer and four chemical shift for the ring protons of DMAP in the *cis* isomer. No change of isomer ratio was observed after cooling to – 55°C nor after heating at 50 °C for 1h. These assignments were confirmed by a COSY study (see S37a). ^{13}C NMR are consistent with the presence of isomeric structures and contains signals from two CO carbons; COSY, NOESY and HMQC spectra were measured to complete this assignment. These isomers are not in equilibrium on the proton NMR time scale but they are formed in slightly different mole ratio in repeated synthetic experiments. Both cooling to -55°C and heating of the NMR tube containing both isomers for 1 h at 50°C show no changes in relative intensities of isomer signals. Two kinetic isomers probably arise because CO attacks an unsaturated LFe(DMAP)$_2$ complex that is in fast, unfavorable equilibrium with LFe(DMAP)$_3$ and formation of *trans* and *cis* isomers is the result of CO attack to meridional and apical positions, respectively. Seeking evidence for two isomers by infrared spectroscopy, we observe only one, but broadened, signal at 1963 cm^{-1} in dichloromethane. The CO stretching frequencies of two isomers of Ru(terpy)Cl_2(CO)[13] are very similar at 1950 and 1953 cm^{-1}. Thus, the solution composition is more complicated than is indicated by the least soluble isomer which crystallized for the x-ray study.

L^{Me}Fe^{II} complexes with weakly coordinated counterions.

We also considered that perhaps the inability of CO or PEt_3 to cleave $LiClFe_2L_2$ was because the chloride was an especially favorable nucleophile bridging the two LFe^{II} fragments. Our intended test of this was to make a chloride-free analog with the very weakly nucleophilic anion triflate, $CF_3SO_3^{-1}$. We also decided to remove the pyrazole hydrogen bonding functionality, so investigated L^{Me} instead of H_2L as the neutral pincer ligand. We were interested in the impact of double alkylation of L^{2-} β nitrogens on its donor power vs. LFe(DMAP)$_3$. L^{Me} is also desirable because it cannot aggregate by pyrazolate bridging through its β nitrogen. Finally we chose to try to synthesize a dicationic monomer directly, by working in MeCN solvent, as a ligand that failed to react with $LiClFe_2L_2$.

Author Manuscript

This article is protected by copyright. All rights reserved

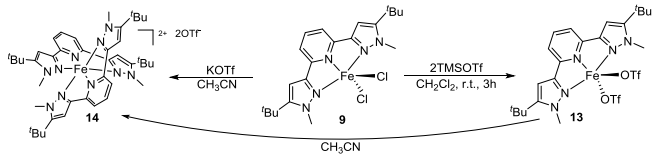

Scheme 11. Ligand redistribution with labile counterion.

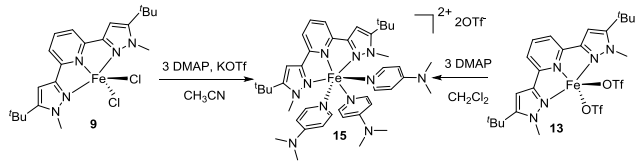

Scheme 12. Formation of cationic complexes with $[(L^{Me})Fe]^{2+}$ fragment.

Treatment of $L^{Me}FeCl_2$ **9** with excess of KOTf in CH_3CN results (Scheme 11) in a rapid color change from orange to yellow; after additional stirring for 3h, all volatiles were removed and the residue was dissolved in dichloromethane and filtered through Celite to remove KCl/KOTf. A yellow powder was obtained, after addition of pentane to concentrated dichloromethane extract, whose ^1H NMR spectra in CD_3CN indicates paramagnetism and shows a pattern of 5 signals with 1:2:2:6:18 relative intensities that is in agreement with C_2 symmetry of the ligand; these chemical shifts are completely different from those of $L^{Me}FeCl_2$. ^{19}F NMR showed a sharp singlet at -78 ppm that proves the presence of *free* OTf^- counterion. Mass spectroscopy shows the ions 379.3 and 907.1 m/z in APCI+ that correspond to $[(L^{Me})_2Fe]^{2+}$ and $[(L^{Me})_2Fe](OTf)^+$, respectively, establishing the formation of a *bis*-pincer adduct.

To compare the above synthesis in the *absence* of a coordinating solvent, we treated $L^{Me}FeCl_2$ with 2 eq of Me_3SiOTf in CH_2Cl_2, which results (Scheme 11) in immediate bleaching from orange to lemon-yellow; after concentration and addition of pentane a yellow precipitate was formed. ^1H NMR of the obtained solid shows a pattern of 5 signals in a range from -32 to +61 with 1:2:2:6:18 relative intensities. These ^1H NMR chemical shifts are very close to those obtained for $L^{Me}FeCl_2$ and very different from signals obtained above for $[(L^{Me})_2Fe]^{2+}$. ^{19}F NMR showed a broad singlet at -16 ppm, whose shift indicates that OTf is interacting with a paramagnetic center. The ESI mass-spectrum shows a signal at 556.0 m/z corresponding to $[L^{Me}Fe(OTf)]^+$.

Dissolving this $L^{Me}Fe(OTf)_2$ in acetonitrile results in immediate color change from lemon-yellow to deep yellow and the isolated product showed ^1H and ^{19}F NMR signals identical to the experiment with KOTf, that product being $[(L^{Me})_2Fe]^{2+}$. This indicates that, in acetonitrile, fast pincer ligand redistribution occurs with formation of $[(L^{Me})_2Fe]^{2+}$ and probably $Fe(NCMe)_6^{2+}$. To prove this pincer product identity, $[(L^{Me})_2Fe]^{2+}(OTf)_2$ was independently synthesized by reacting 2 eq. of L^{Me} with 1 eq. of $Fe(OTf)_2$ in MeCN; the isolated product showed identical ^1H and ^{19}F NMR as $[(L^{Me})_2Fe]^{2+}$ formed above. This indicates a strong tendency of Fe^{2+} to form octahedral complexes and take part in ligand redistribution even with tridentate ligands.

Reaction of $L^{Me}FeCl_2$ in MeCN with excess KOTf the presence of 3 equivalents of DMAP at room temperature (Scheme 12) leads to a dark orange solution within 10 min of mixing.

Filtration and removal of volatiles yields an orange powder that was recrystallized from CH_2Cl_2/pentane. The ^1H NMR spectrum of this species in $CDCl_3$ reveals the molecule to be *paramagnetic*, with proton chemical shifts from -12 to 62 ppm. ^{19}F NMR, a broad line at 60 ppm, indicates the presence of triflate counterions, but free triflate would appear at 78 ppm; the observed broadness and 18 ppm downfield shift of this ^{19}F NMR signal indicates that triflate is involved in a fast exchange process with DMAP ligands, or shows intimate ion pairing of triflate with the paramagnetic dication. APCI MS showed a positive ion m/z = 923.4, due to the ion pair $[L^{Me}Fe(DMAP)_3(OTf)]^+$.

Single crystal X-ray diffraction (Figure 10) confirms the formula $L^{Me}Fe(DMAP)_3^{2+}$ with noninteracting triflate counter ions. Of the six Fe/N distances, those to N-methylpyrazole are longest, those to pincer pyridine shortest, and those to DMAP are intermediate. All are significantly longer in comparison to those in $LFe(DMAP)_2(CO)$, consistent with a high spin d^6 configuration for this L^{Me} species. In spite of the unique DMAP being imperfectly aligned angularly (angle Fe-N6-*para*C = 167.9°), its Fe-N distance is not unusually long. All NMe_2 groups are planar and eclipse the ring planes, for best π donation.

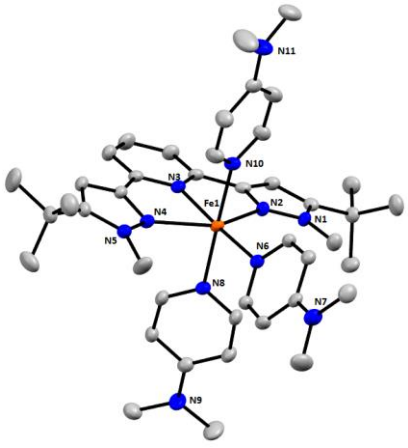

Figure 10. Mercury drawing of the nonhydrogen atoms of the cation in $[L^{Me}Fe(DMAP)_3](triflate)_2$, showing selected atom labelling; unlabeled atoms are carbon, and dichloromethane and triflates are omitted for clarity. Selected structural parameters: Fe1-N2, 2.256(2) Å; Fe1-N3, 2.165(2); Fe1-N4, 2.266(2); Fe1-N6, 2.207(2); Fe1-N8, 2.165(2); Fe1-N10, 2.200(2).

Attempts to react $[(L^{Me})Fe(DMAP)_3]^{2+}(OTf)_2$ with excess CO at 1 atm. at 25°C showed no reaction by both NMR and IR spectra indicating no reactivity.

Author Manuscript

This article is protected by copyright. All rights reserved

Conclusions

We have shown (Scheme 1) that $LiN(SiMe_3)_2$ reacts with $(H_2L)MCl_2$ to give $LiClM_2L_2$, thus some chloride is retained by the metal, in order to avoid low metal coordination number: the metal in hypothetical dimeric M_2L_2 is significantly Lewis acidic. The collective evidence from these studies shows that divalent iron is not strongly obedient to the 18 electron rule, although Fe^{II} is faithful to preferred coordination number 6; among all species reported here, only the Fe_2 and Fe_3 species have coordination number 5, in the frequently populated Fe_2L_2X structure shown in Scheme 1. Already the abundant evidence that divalent iron with six ligands and octahedral geometry is nearly thermo-neutral between high-spin and low-spin alternatives ("spin crossover")[1a, 12] shows the lack of a strong energetic preference for any one *electronic* structure. Since the high spin alternative invariably populates orbitals which are maximally sigma antibonding between metal and ligand, the corollary observation from our results of dissociative intermediates (hence higher energy) becomes understandable. Even when the isolated species is six coordinate, ligand substitution reactions have a facile mechanism, based upon easy dissociation of one ligand, followed by addition of the new ligand. Taken together, this shows both the complexity of substitution chemistry of divalent iron, yet leaves open abundant opportunities for low barrier substrate binding for achieving equilibrium population of product adduct.

The collective results here show pincer ligand influence on spin state. Doubly alkylated $L^{Me}Fe(DMAP)_3^{2+}$ is exclusively high spin while $LFe(DMAP)_3$ shows spin equilibrium, showing L^{Me} to be a weaker donor. The curious lack of reaction of $L^{Me}Fe(DMAP)_3^{2+}$ with CO, contrasting to ready carbonylation of $LFe(DMAP)_3$ must originate in weak donation by L^{Me} causing iron to bind DMAP tighter, thus making kinetic access to the dissociative intermediate $L^{Me}Fe(DMAP)_2^{2+}$ difficult, as well as bad enthalpy of formation of unobserved $L^{Me}Fe(DMAP)_2(CO)^{2+}$.

Replacing one DMAP in $LFe(DMAP)_3$ by a single CO converts an S = 2 species into an S = 0 ground state, an impressive accomplishment by changing only *one* ligand. We suggest that a single ligand can do this by, along the Fe-C line, not only raising the $d\sigma$ orbital but stabilizing (back donation) two $d\pi$ orbitals which collectively lead to preference for all electrons in the $d\pi$ orbitals. However, given the fact that low and high spin isomers are in thermal equilibrium (hence low ΔG^o and low barrier for equilibration) for complexes *not* incorporating strong π acids (*e.g. not* CO), the need to convert a high spin reagent (THF, DMAP) to a low spin carbonyl product, as observed here, cannot have a high thermodynamic penalty. Others have observed weak CO binding in divalent iron carbonyl complexes, but without clear explanations of their cause[14]

For example, why is $L^{Me}Fe(DMAP)_3^{2+}$ inert to 1 atm CO? The origin of the puzzling weak Fe/C bond strength in high spin iron complexes must lie in other causes than simple "spin crossover"[12] or "spin forbiddenness," such as ineffective π basicity of the metal in the resulting low spin carbonyl complexes. Perhaps back donation from Fe^{2+} to CO is poor due to the contracted d orbitals.

Formation of *bis*-pincer dication here cannot be prevented under the same condition by addition of 3 eq of Et_3P or 1 atm of CO. Only ligands that can break aggregates of LFe can stabilize mono-pincer cationic complexes of $L^{Me}Fe$. $[(L^{Me})_2Fe]^{2+}$ is apparently a thermodynamic minimum for all equilibrium ligand exchange processes in polar solvent and establishes a tendency of Fe^{2+} to form the *bis*-pincer octahedral complex; we find that $[(L^{Me})_2Fe]^{2+}$, once formed, is not cleaved open to $(L^{Me})Fe(\text{Lewis base})_n^{2+}$ by PEt_3 or CO.

Experimental Section

General. All manipulations were carried out under an atmosphere of ultra high purity nitrogen using standard Schlenk techniques or in a glovebox under argon. Solvents were purchased from commercial sources, purified using Innovative Technology SPS-400 PureSolv solvent system or by distilling from conventional drying agents and degassed by the freeze-pump-thaw method twice prior to use. Glassware was oven-dried at 150 °C overnight and flame dried prior to use. THF, including d_8-THF was stored over activated 4 Å molecular sieves or sodium metal pieces. The synthesis of ligand LH_2 has been reported.[15] All reactions were performed in a MBraun Lab Master 130 glovebox under N_2 atmosphere or with a Schlenk line using standard techniques. Commonly used laboratory solvents were obtained from an Innovative Technology SPS-400 PureSolv solvent purification system and stored with activated molecular sieves. THF and benzene were additionally stored over Na metal prior to use. Deuterated and uncommon solvents were dried with CaH_2 for ca. 12h before undergoing vacuum transfer through standard "freeze-pump-thaw" techniques and stored over molecular sieves prior to use. DMAP, dppe, $LiN(TMS)_2$, $FeCl_2$ were purchased from commercial sources and used without further purification. All ^1H and ^{31}P NMR spectra were collected using a Varian Inova 400 MHz spectrometer. ^1H NMR spectra of paramagnetic compounds were collected with acquisition time of 0.1- 0.4s and 0.01 s relaxation delay and at least 2048 transients per spectra. ^1H NMR spectra are referenced vs. respective protio impurities of solvents employed (e.g. C_6D_5H). ^{31}P NMR are referenced vs. H_3PO_4 @ 0.00 ppm. Mass spectrometric analyses were performed in an Agilent 6130 MSD (Agilent Technologies, Santa Clara, CA) quadrupole mass spectrometer equipped with a Multimode (ESI and APCI) source. Cyclic voltammetry was done with Pt as the working electrode, Pt as the counter electrode, and Ag/AgCl wire as the reference electrode. 0.1M $TBAPF_6$ was employed as a supporting electrolyte, in THF solvent. In this medium, ferrocene has a peak-to-peak separation of ~0.50V. 13.5 and 15.5mg of free ligand and Fe complex were used, respectively, in 10 mL solvent. All CVs are referenced to internal Fc/Fc^+ as the standard, added at the end of a study of the experimental sample. Electrodes were polished when a new molecule was studied. We designate "open circuit potential" as the potential where there is negligible current flow for the species dissolved. H_2LFeCl_2 (**1**) and $L^{Me}FeCl_2$ (**9**) were synthesized according to literature[2b, 16].

Compound 2 ($LiClFe_2L_2$): A 100 mL round-bottom Schlenk flask was charged with 592 mg (1.313 mmol) $(H_2L)FeCl_2$ and dissolved in 25 mL THF. To this was added a solution of 450 mg (2.69 mmol) $LiN(TMS)_2$ dissolved in 15 mL THF. Upon addition, a slight color change from red to darker red-orange was observed. The final mixture was allowed to stir for 12 h at room temperature without further color change or precipitation. Volatiles were removed under reduced pressure, and the resulting orange solid was extracted with 20 mL toluene. The resulting orange slurry was filtered through a medium porosity ground-glass frit to remove a white solid and the dark red-orange filtrate was collected. Volatiles were once again removed from the filtrate under reduced pressure to

Author Manuscript

This article is protected by copyright. All rights reserved

yield an orange solid. This orange solid was dissolved in the minimum amount of toluene (~10 mL) and precipitated with 90 mL pentane. The resulting slurry was filtered through a medium porosity frit and the orange solid on the frit was collected and dried in vacuo. The filtrate was collected and stripped to dryness; the resulting solid was extracted into 2 mL toluene and 50 mL of pentane was added, and the resulting additional resulting orange solid was collected and added to the initial crop. The resulting filtrate here was discarded. Yield: 406 mg (77%). Single crystals suitable for X-ray diffraction were obtained from slow vapor diffusion of pentane into a saturated benzene solution. ^{1}H NMR (400 MHz, d8-THF, 25^{o}C): δ(ppm) 89.8(2H), 81.0(2H), 80.2(2H), 26.4(2H), 9.86(2H), 3.63(18H), -7.21(18H). FT-IR (KBr, CH_2Cl_2)**: (cm^{-1})** 1606, 1571 (see S.I. for full spectrum).

Compound 3 ($H_2Na_4Fe_3L_5O$): 200 mg (0.62 mmol) of LH_2 was dissolved in 5 mL Et_2O and this was added to a stirring slurry of excess NaH (60 mg) in Et_2O, which resulted in immediate vigorous bubbling. This mixture was allowed to stir at room temperature until the evolution of bubbling ceased. This mixture was then filtered through a Celite plug and simultaneously dropwise added to a stirring slurry of 80 mg (0.63 mmol) anhydrous $FeCl_2$ slurried with 10 mL Et_2O in a separate 20 mL scintillation vial. The resultant addition turned the beige $FeCl_2$ to orange, however the solution remained heterogeneous. The final mixture was allowed to stir at room temperature for 12 h, which resulted in no further color change or appearance of the solution. The solid in the mixture was allowed to settle, which revealed a deep orange-red supernatant and gray solid. This gray solid was removed via filtration through a Celite plug and the red-orange supernatant collected. Volatiles were removed under reduced pressure and the resulting orange solid extracted into toluene. The toluene solution was then filtered again and volatiles removed under reduced pressure to yield and analytically pure orange solid. Single crystals suitable for X-ray diffraction can be grown from a saturated benzene solution. ^{1}H NMR(C_6D_6, 400 MHz, 298K): δ (ppm) 39.9(2H), 34.7(2H), 30.9(2H), 28.1(2H), 25.1(2H), 20.9(2H), 14.8(2H), 11.3(2H), 9.10(2H), 7.96(2H), 6.10(2H), 5.57(2H), 3.02(18H), 0.67(18H), 0.56(18H), 0.27(18H), -0.08(18H), -2.08(1H), -5.41(2H).

Compound (4) ($[(H_2L)Fe(THF)_3](BArF_4)_2$): 100 mg (0.22 mmol) $(H_2L)FeCl_2$ was dissolved with 6 mL THF in a 20 mL scintillation vial. To this was added 400 mg (0.45 mmol) $NaBArF_4$ dissolved in 6 mL of THF dropwise via glass pipette over the course of 5 min at room temperature. Color change from orange-red was observed during the addition of $NaBarF_4$ to a golden yellow solution with a simultaneous increase in turbidity. The mixture was allowed to stir vigorously for 1 h with no further color change. The reaction mixture was filtered through Celite and volatiles removed from the filtrate under reduced pressure to yield a yellow solid. This solid was extracted with 3 x 5 mL of toluene and the undissolved solid was again dried under reduced pressure which resulted in an analytically pure yellow powder. Single crystals were obtained from layering pentane onto a saturated THF solution at -35^{o}C. ^{1}H NMR (THF-D_8, 400 MHz, 25^{o}C) δ(ppm): 58.6(2H), 44.4(2H), 33.8(2H, NH), 7.74(s, Ar-o $BArF_4$, 16H), 7.52(s, Ar-p $BArF_4$), 8H), 2.65(18H). ^{19}F NMR (CD_2Cl_2, 376.5 MHz, 25^{o}C) δ(ppm): -64.1 ($BArF_4$). ESI-MS(+) m/z (in THF): 298.1=$(H_2L)Fe(THF)_3^{2+}$ Calc for $C_{31}H_{49}FeN_5O_3$: 297.7. Single crystals were obtained from layering pentane onto a saturated CH_2Cl_2 solution at -35^{o}C. Space group P-1, a = 13.9409(5) Å, b = 14.3255(9), c = 26.0405(9), α = 85.361(3)^{o}, β = 87.6790(2), γ = 88.1910(10), V = 5177.22 Å^3.

Compound 5 ($[(H_2L)Fe](BArF_4)_2$): This product was isolated via the same reaction conditions as described above, however crystals were grown from slow diffusion of pentane into a saturated CH_2Cl_2 solution at -35^{o}C. ^{1}H NMR (CD_2Cl_2, 400 MHz, 25^{o}C) δ(ppm): 59.2(2H), 52.0(2H), 33.1(2H), 22.7(1H), 7.72(s, Ar-o $BArF_4$, 16H), 7.53(s, Ar-p $BArF_4$), 8H), 1.28(18H). ^{19}F NMR (CD_2Cl_2, 376.5 MHz, 25^{o}C) δ(ppm): -62.7 ($BArF_4$).

Compound 6a [(L)Fe(κ^2-dppe)(κ^1-dppe)]: To a 100 mL round bottom flask was slurried 400 mg (0.887 mmol) $(LH_2)FeCl_2$ in 20 mL of Et_2O. To this slurry was added 710 mg (1.78 mmol) dppe and the new mixture stirred for an additional 20 min with no observed color change. To this was added dropwise a solution of 300 mg (1.79 mmol) $LiN(TMS)_2$ dissolved in 5 mL Et_2O over the course of 5 min. The final mixture was allowed to stir for 12 h, upon which a final dark orange/red solution color was observed. The resulting gray precipitate was filtered through a medium porosity ground glass frit and the filtrate collected. Removal of volatiles from the pentane filtrate resulted in a thick orange oil. This orange oil was extracted with pentane, and filtered again through a ground glass frit of medium porosity and the filtrate collected. Removal of volatiles resulted in an analytically pure lustrous dark orange solid. Single crystals can be grown by slow evaporation of a concentrated pentane solution at -35^{o}C. ^{1}H NMR(C_6D_6, 400 MHz, 298 K): 8.64(dd, 4H, dppe Ar-ortho, $^{3}J_{HP}$ = 12.0 Hz, $^{3}J_{HH}$ = 8.0 Hz), 7.32(m, 2H, dppe-Ar), 7.19(t, 1H, pyridyl Ar-para, $^{3}J_{HH}$ = 8.0 Hz), 7.17(m, 2H, dppe-Ar), 7.13(d, 4H, dppe Ar-meta, $^{3}J_{HH}$ = 8.0 Hz), 7.09(d, 2H, dppe-Ar, $^{3}J_{HH}$ = 8.0 Hz), 7.02(m, 2H, dppe-Ar, $^{3}J_{HH}$ = 2.8 Hz), 6.94(q, 4H, dppe-Ar, $^{3}J_{HH}$ = 8.0 Hz), 6.87(t, 4H, dppe-Ar, $^{3}J_{HH}$ = 8.0 Hz), 6.82(t, 4H, dppe-Ar, $^{3}J_{HH}$ = 8.0 Hz), 6.72(q, 8H, dppe-Ar, $^{3}J_{HH}$ = 8.0 Hz), 6.38(d, 2H, Py Ar-meta, $^{3}J_{HH}$ = 8.0 Hz), 6.34(t, 4H, dppe-Ar-ortho, $^{3}J_{HH}$ = 8.0 Hz, $^{3}J_{HP}$ = 8.0 Hz), 6.21(s, 2H, Pz-CH, 2H), 3.60(dq, 2H, dppe-CH_2, $^{2}J_{HP}$ = 16.0 Hz, $^{3}J_{HH}$ = 8.0 Hz), 1.97(dq, 2H, dppe-CH_2, $^{2}J_{HP}$ = 16.0 Hz, $^{3}J_{HH}$ = 8.0 Hz), 1.75(br, 4H, dppe-CH_2), 1.71(s, 18H, ^{t}Bu). ^{13}C NMR(C_6D_6, 101 MHz, 298 K): 165.8(s), 156.1(s), 152.7(d, J_{PC} = 3.0 Hz), 139.3(d, J_{PC} = 17.2 Hz), 139.2(d, $^{1}J_{PC}$ = 28.3 Hz), 136.7(d, $^{1}J_{PC}$ = 30.3 Hz), 136.0(d, J_{PC} = 10.1 Hz), 133.5(d, J_{PC} = 8.1 Hz), 133.3(d, J_{PC} = 18.2 Hz), 133.2(d, J_{PC} = 4.0 Hz), 133.1(d, J_{PC} = 9.1 Hz), 132.5(s), 132.3(d, J_{PC} = 9.1 Hz), 129.0(d, J_{PC}, 2.0 Hz), 128.8(t, J_{PC} = 3.0 Hz), 128.5(d, J_{PC} = 7.1 Hz), 128.4(s), 127.9(s), 127.6(dd, J_{PC} = 9.1 Hz, J_{PC} = 11.1 Hz), 127.4(d, J_{PC} = 8.1 Hz), 111.2(s), 99.8(s), 34.8(dd, $^{1}J_{PC}$ = 26.8 Hz , $^{2}J_{PC}$ = 16.2 Hz), 32.9(s), 32.3(s), 28.9(dd, $^{1}J_{PC}$ = 24.2 Hz , $^{2}J_{PC}$ = 12.1 Hz), 23.9(dd, $^{1}J_{PC}$ = 16.2 Hz, $^{2}J_{PC}$ = 8.1 Hz), 19.3(dd, $^{1}J_{PC}$ = 25.3 Hz , $^{2}J_{PC}$ = 12.1 Hz). ^{31}P NMR(C_6D_6, 161.97 Hz, 298 K): δ(ppm) 67.6 (dd, 1P, $^{2}J_{P\text{-}P}$ = 45.3 Hz, $^{3}J_{P\text{-}P}$ = 25.19 Hz), 63.9 (dd, 1P, $^{2}J_{P\text{-}P}$ = 136.1 Hz, $^{3}J_{P\text{-}P}$ = 25.19 Hz), 46.3 (ddd, 1P, $^{2}J_{P\text{-}P}$ = 136.1 Hz, $^{2}J_{P\text{-}P}$ = 45.3 Hz, $^{3}J_{P\text{-}P}$ = 26.9 Hz), -11.7 (d, 1P, $^{3}J_{P\text{-}P}$ = 26.9 Hz). ESI-MS(+): m/z, calc. for $C_{45}H_{47}FeN_2P_2$ = 775.27, found = 775.3, $[LFe(dppe)]^{+}$.

Compound 6b ($[[LFe(κ^2\text{-}dppe)]_2(μ\text{-}dppe)$): This is in the pentane insoluble residue after thorough extraction of (L)Fe(κ^2-dppe)(κ^1-dppe) from any reaction product. ^{31}P NMR(C_6D_6, 162 MHz, 298 K): δ(ppm) 65.9(dd, 2P, $^{2}J_{pp}$ = 43.7 Hz, $^{3}J_{PP}$ = 22.7 Hz), 61.9(dd, 2P, $^{2}J_{PP}$ = 130.4 Hz, $^{3}J_{PP}$ = 22.7 Hz), 40.0(dd, 2P, $^{2}J_{PP}$ = 130.4 Hz, $^{3}J_{PP}$ = 43.7 Hz).

Compound 7 (L)Fe(^{t}BuNC)$_3$: A 20 mL scintillation vial was charged with 100 mg (0.222 mmol) $(LH_2)FeCl_2$ and slurried in 10 mL Et_2O. To this was added 76 μL (0.672 mmol) ^{t}BuNC which resulted in no observable color change. To this mixture, a 5 mL solution of 80 mg (0.478 mmol) $LiN(TMS)_2$ in Et_2O was added dropwise over the course of 60 seconds and a rapid color change to orange-yellow was observed. The reaction mixture was allowed to stir at room temperature for 2 h, upon which an increased turbidity was observed. The mixture was filtered through a Celite plug and the filtrate collected and volatiles removed under reduced pressure. The resulting orange oil was extracted 3 x 5 mL of pentane and filtered again through Celite, and the orange-yellow filtrate collected. Volatiles were removed under reduced pressure to yield an analytically pure orange-yellow solid. Yield: (84%). ^{1}H NMR(C_6D_6, 400 MHz, 298 K): δ(ppm) 7.29(t, 1H, Ar-p, $^{3}J_{HH}$ 8.0 Hz), 7.04(d, 2H, Ar-m, $^{3}J_{H\text{-}H}$ 8.0 Hz), 6.77(s, 2H, pz-CH), 1.61(s, 18H, $C(CH_3)_3$), 1.50(s, 9H, $C(CH_3)_3$), 0.58(s, 18H, $C(CH_3)_3$). ^{13}C NMR(C_6D_6, 101 MHz, 298 K): δ(ppm) 173.1, 165.3,

Author Manuscript

This article is protected by copyright. All rights reserved

156.1, 149.7, 136.1, 110.3, 98.4, 57.3(1C, CN*C*$(CH_3)_3$), 56.3(2C, *trans*-CN*C*$(CH_3)_3$), 32.7(2C, Pz-*C*$(CH_3)_3$), 31.6(6C, C(CH_3)$_3$), 30.7(3C, CNC(CH_3)$_3$), 29.54(6C, *trans*-CNC(CH_3)$_3$. FT-IR(pentane solution): υ(cm^{-1}) 2157(m), 2131(vs), 2078(m). ESI-MS(+) m/z: calc for $C_{34}H_{51}FeN_8^+$ 627.36. Found: 627.4. Calc for $C_{39}H_{60}FeN_9^+$ 710.43. Found: 710.5. All other expected isotopomers for ^{54}Fe, ^{13}C, ^{15}N, and ^{57}Fe were also observed (see S.I.).

Compound 8 ([L^{Me}Fe(^{t}BuNC)$_3$](BF$_4$)$_2$): 40.0 mg (0.064 mmol) LFe(^{t}BuNC)$_3$ was dissolved in 1.0 mL CH_2Cl_2 and this was added to 24.0 mg (0.16 mmol) of Me_3OBF_4. The resulting slurry was allowed to stir for 2 h at room temperature, during which a color change from yellow to orange-red was observed, but excess solid Me_3OBF_4 remained. The resulting orange solution was decanted away from the solids and volatiles removed under reduced pressure to yield an analytically pure orange solid. Yield: 93%. The other 7% is [(H_2L)Fe(^{t}BuNC)$_3$](BF$_4$)$_2$, identified by ^{1}H NMR spectroscopy, which is the result of HBF_4 impurity in the alkylating reagent. Single crystals suitable for X-ray diffraction were obtained by slow evaporation of a concentrated CH_2Cl_2 solution ^{1}H NMR (CD_2Cl_2, 400 MHz, 298 K): δ(ppm) 8.38(t, Ar-p, 1H, $^3J_{HH}$ = 8.0 Hz), 8.10 (d, Ar-m, 2H, $^3J_{HH}$ = 8.0 Hz), 6.88 (s, 2H, Pz-CH), 3.86(s, 6H, N-Me), 1.87 (s, 9H, CNC(CH_3)$_3$), 1.40 (s, 18H, *trans*-CNC(CH_3)$_3$), 1.27 (s, 18H, Pz-C(CH_3)$_3$). ^{13}C NMR (CD_2Cl_2, 100.6 MHz, 298K): δ(ppm) 161.6, 153.0, 151.6, 141.1, 120.2, 104.5, 62.0, 60.3, 40.2, 32.8, 30.41, 30.39, 29.3, 27.0. ^{19}F NMR (CD_2Cl_2, 376.5 Hz, 298 K): δ(ppm) -149.5 (s, br). FT-IR (CH_2Cl_2): υ(cm^{-1}): 2205(m), 2178(vs), 2164(s). ESI-MS(+): m/z; calc. for $C_{46}H_{56}BF_4FeN_8$ = 743.4, observed = 743.3, [L^{Me}Fe(^{t}BuNC)$_3$](BF$_4$)$^+$.

Compound 10 (L^{Me}Fe(^{t}BuNC)$_2$): A 20 mL scintillation vial was charged with [L^{Me}Fe(^{t}BuNC)$_3$](BF$_4$)$_2$ (80.0 mg, 0.100 mmol) dissolved in 10 mL THF and a Pyrex-covered magnetic stir bar, resulting in a pale orange/pink solution. To this was added excess KC_8 (41.0 mg, 0.303 mmol) and the reaction mixture immediately turned dark. The mixture was allowed to stir at r.t. for an additional 2 h. After filtration through Celite to remove graphite, a dark orange filtrate was obtained, from which volatiles were removed under reduced pressure. The resulting dark orange tacky solid was extracted into 10 mL toluene and again filtered through Celite. Removal of volatiles from the filtrate under reduced pressure resulted in a spectroscopically pure dark orange powder. ^{1}H NMR (C_6D_6, 400 MHz, 298 K): δ(ppm), 8.28(d, 2H, Ar-m, $^3J_{HH}$ = 7.6 Hz), 7.35(t, 1H, Ar-p, $^3J_{HH}$ = 7.6 Hz), 7.25(s, 2H, pz-CH), 3.55(s, 6H, N-CH_3), 1.22(s, 18H, tBu), 1.08(s, 18H, tBu). FT-IR(KBr, C_6H_6): ν(cm^{-1}): 2017(s), 2145(vs)

Compound 11 [(L)Fe(DMAP)$_3$]: A 100 mL round-bottom flask was charged with 300 mg (0.665 mmol) (LH_2)$FeCl_2$ and 30 mL toluene. To this stirring slurry was added 225 mg (1.34 mmol) LiN(TMS)$_2$ dropwise in 5 mL toluene with color change from pale yellow to orange. To this resulting slurry was added 245 mg (2.00 mmol) of DMAP in 5 mL toluene resulting in an immediate color change to deep red. The final mixture was allowed to stir for an additional 12 h with no further change in color. The precipitate was allowed to settle and removed via filtration through a ground glass frit of medium porosity resulting in a deep red filtrate. Volatiles were removed under reduced pressure to yield a red-brown solid. Yield: 453 mg (92%) Single crystals suitable for X-ray diffraction were grown by slow evaporation of a saturated benzene solution at 25°C. ^{1}H NMR(C_6D_6, 400 MHz, 25°C): δ(ppm) 44.8(2H), 38.3(1H), 30.6(2H), 15.5(6H), 8.15(4H), 4.53(18H), 3.58(2H), 3.09(12H), -9.71(2H). Evans method magnetic susceptibility determination (C_6D_6, vs. C_6Me_6, 400 MHz, 25°C): 4.6 μ_B (4.5 μ_B in second determination). APCI-MS(-): m/z calc for $C_{38}H_{47}FeN_{10}$ (M-N(CH_3)$_2$)$^{-1}$. 699.3. Found: 698.3. The molecule crystallizes with benzene guest molecules, but these show no clear pi stacking with any rings of the coordination complex.

Compound 12 [(L)Fe(DMAP)$_2$(CO)]: LFe(DMAP)$_3$ (19 mg, 0.026 mmol) was dissolved in 0.5 ml of appropriate deuterated solvent solvent (benzene, toluene or dichloromethane) and transferred in to J. Young NMR tube. The tube was degassed three times by pump-thaw operations and 190 Torr (1 eq.) of CO was added to a frozen solution of the complex. The tube was warmed to room temperature and shaken intensively for 1 min, resulting in a color changed from deep red to orange in 1 min and formation of orange precipitate. After 1 h, the solution was transferred to a 5 mL scintillation vial and 2 mL of pentane was added to cause additional precipitation. The mother liquor was decanted and the yellow-orange powder was washed twice with pentane. Yield: 90%. Red crystals suitable for X-ray diffraction were grown by slow diffusion of pentane vapors in concentrated solution in CD_2Cl_2. *0.8:1 cis/trans ratio. trans*-LFe(DMAP)$_2$CO: ^{1}H NMR (400 MHz, CD_2Cl_2, 298 K, ppm): δ = 1.38 (s,18H, *t*-Bu), 2.74 (s, 12H, NMe_2), 5.90 (d, 2H, J_{HH} = 6.3 Hz, *meta*-DMAP), 6.55 (d, 2H, J_{HH} = 6.3 Hz, *ortho*-DMAP), 6.64 (s, 2H, 4-pyrazole), 7.31 (d, 2H, J_{HH} = 7.3 Hz, *meta*-Lpyridine), 7.81 (t, 1H, J_{HH} = 7.3 Hz, *para*-Lpyridine); *cis*- LFe(DMAP)$_2$CO: ^{1}H NMR (400 MHz, CD_2Cl_2, 298 K, ppm): δ = 1.37 (s,18H, *t*-Bu), 2.83 (s, 6H, *axial*-NMe_2), 3.04 (s, 6H, *equat*-NMe_2), 6.16 (d, 2H, J_{HH} = 6.4 Hz, *axial-meta*-DMAP), 6.56 (d, 2H, J_{HH} = 6.4 Hz, *equat-meta*-DMAP), 7.04 (d, 2H, J_{HH} = 7.4 Hz, *meta*-Lpyridine), 7.15 (d, 2H, J_{HH} = 6.4 Hz, *axial-ortho*-DMAP), 7.36 (s, 2H, 4-pyrazole), , 7.52 (t, 1H, J_{HH} = 7.4 Hz, *para*-Lpyridine), 9.28 (d, 2H, J_{HH} = 6.4 Hz, *equat-ortho*-DMAP); *cis/trans*- LFe(DMAP)$_2$CO: ^{13}C NMR (400 MHz, CD_2Cl_2, 298 K, ppm): δ = 30.8 ((*C*H_3)$_3$C), 31.0 ((*C*H_3)$_3$C), 32.3 ((CH$_3$)$_3$*C*), 32.4 ((CH$_3$)$_3$*C*), 38.5 (N(*C*H$_3$)$_2$), 38,7 (N(*C*H$_3$)$_2$), 38.8 (N(*C*H$_3$)$_2$), 98.8, 99.6, 106.7, 111.1, 112.2, 128.3, 138.4, 150.0, 150.6 151.5, 151,7, 153.6, 155.6, 156.0, 156.2, 165.3, 168.3, 207.7 (*C*O), 212.9 (*C*O); IR (CD_2Cl_2, cm^{-1}): *v* = 1963 cm^{-1}.

Compound 13 [(LMe)Fe(OTf)$_2$]: $L^{Me}FeCl_2$ (49 mg, 0.1 mmol) was dissolved in 5 mL of dichloromethane followed by addition of 2 eq of TMSOTf. The reaction mixture turns light-yellow immediately and was stirred for additional 12 h. Volatiles were removed under vacuum and the product was redissolved with CH_2Cl_2 (15 mL), filtered through Celite, concentrated up to 3 mL and pentane was added to cause precipitation of yellow powder. Yield: 95%. **^{1}H NMR (400 MHz, CD_2Cl_2, 298 K, ppm):** δ = 61.20 (s, 2H), 45.89 (s, 2H), 13.01 (s, 6H), 6.71 (s, 18H), -23.01 (s, 1H). **^{19}F NMR (376.5 MHz, CD_2Cl_2, 298 K, ppm):** δ = -16.3 (s). **MS (APCI)** m/z = 556.0 m/z [L^{Me}Fe(OTf)]$^+$.

Compound 14 [(L^{Me})$_2$Fe](OTf)$_2$]: L^{Me} (70 mg, 0.2 mmol) and Fe(OTf)$_2$ (35 mg, 0.1 mmol) were dissolved in 5 mL of CH_3CN. Reaction mixture turns deep yellow immediately and was stirred for additional 12 h. Volatiles were removed under vacuum and the product was redissolved with CH_2Cl_2 (15 ml), filtered through Celite, concentrated up to 3 mL and pentane was added to cause precipitation of yellow powder. Yield 92%. **^{1}H NMR (400 MHz, CD_2Cl_2, 298 K, ppm):** δ = 61.81 (s, 2H), 52.04 (s, 2H), 23.61 (s, 1H), 5.88 (s, 18H), -11.55 (s, 6H). **^{18}F NMR (376.5 MHz, CD_2Cl_2, 298 K, ppm):** δ = -78.1 (s). **MS (ESI+)** m/z = 379.3 [(L^{Me})$_2$Fe]$^{2+}$, 907.1 [(L^{Me})$_2$Fe](OTf)$^+$

Compound 15 [(L^{Me})Fe(DMAP)$_3^{2+}$(OTf)$_2$]: $L^{Me}FeCl_2$ (49 mg, 0.1 mmol) was dissolved in 10 mL of MeCN followed by addition of 3 equiv. of DMAP (37 mg, 0.3 mmol) and 100 mg of KOTf. The reaction mixture turned yellow in 10 min and was stirred for additional 12 h. Volatiles were removed under vacuum and the product was extracted with CH_2Cl_2 (15 ml), filtered through Celite, concentrated to 3 mL and pentane was added caused precipitation of yellow powder. Yield 85%. ^{1}H NMR (400 MHz, CD_2Cl_2, 298 K, ppm): δ = 62.42, 58.04, 51.94, 46.65, 43.73, 23.01, 9.97, 9.94, 9.65, 7.06, 6.63, 6.58, 6.56, 6.54, 5.96, -0.01, -6.02, -11.46. ^{19}F NMR (376.5 MHz, CD_2Cl_2, 298 K, ppm): δ = -60.3. MS (APCI+) m/z = 923.4 [L^{Me}Fe(DMAP)$_3$(OTf)]$^+$

Author Manuscript

This article is protected by copyright. All rights reserved

Acknowledgements

This work was supported by the National Science Foundation, Chemical Synthesis Program (SYN), by grant CHE-1362127. We thank Prof. G. Aromí (U. Barcelona) for SQUID susceptibility determination on $LFe(DMAP)_3$.

Keywords: Iron • Pincer Ligands • Ligand Effects • Lewis Acids • Nitrogen Heterocycles

[1] a) M. A. Halcrow, *Coord. Chem. Rev.* **2005**, *249*, 2880-2908; b) L. T. Ghoochany, S. Farsadpour, Y. Sun, W. R. Thiel, *Eur. J. Inorg. Chem.* **2011**, *2011*, 3431-3437; c) A. Yoshinari, A. Tazawa, S. Kuwata, T. Ikariya, *Chem. – Asian J.* **2012**, *7*, 1417-1425; d) M. A. Halcrow, *Dalton Trans.* **2009**, 2059-2073; eK. Umehara, S. Kuwata, T. Ikariya, *J. Am. Chem. Soc.* **2013**, *135*, 6754-6757.

[2] a) K. G. Caulton, *Eur. J. Inorg. Chem.* **2012**, *2012*, 435-443; b) B. J. Cook, C.-H. Chen, M. Pink, R. L. Lord, K. G. Caulton, *Inorg. Chim. Acta* **2016**, *451*, 82-91.

[3] K. Umehara, S. Kuwata, T. Ikariya, *Inorg. Chim. Acta* **2014**, *413*, 136-142.

[4] a) Y. M. Badiei, W.-H. Wang, J. F. Hull, D. J. Szalda, J. T. Muckerman, Y. Himeda, E. Fujita, *Inorg. Chem.* **2013**, *52*, 12576-12586; b) C. M. Conifer, D. J. Law, G. J. Sunley, A. Haynes, J. R. Wells, A. J. P. White, G. J. P. Britovsek, *Eur. J. Inorg. Chem.* **2011**, *2011*, 3511-3522; c) I. Takao, *Bull. Chem. Soc. Jpn.* **2011**, *84*, 1-16; dS. Kuwata, T. Ikariya, *Dalton Trans.* **2010**, *39*, 2984-2992.

[5] a) O. R. Luca, R. H. Crabtree, *Chem. Soc. Rev.* **2013**, *42*, 1440-1459; b) P. J. Chirik, K. Wieghardt, *Science* **2010**, *327*, 794-795; c) Y.-Y. Fang, W.-J. Gong, X.-J. Shang, H.-X. Li, J. Gao, J.-P. Lang, *Dalton Trans.* **2014**, *43*, 8282-8289.

[6] a) P. J. Chirik, *Angew. Chem. Int. Ed.* **2017**, *56*, 5170-5181.; b) B. L. Small, *Acc. Chem. Res.* **2015**, *48*, 2599-2611; c) R. F. Munha, R. A. Zarkesh, A. F. Heyduk, *Dalton Transactions* **2013**, *42*, 3751-3766.

[7] N. Komine, R. W. Buell, C.-H. Chen, A. K. Hui, M. Pink, K. G. Caulton, *Inorg. Chem.* **2014**, *53*, 1361-1369.

[8] a) N. J. Hardman, X. Fang, B. L. Scott, R. J. Wright, R. L. Martin, G. J. Kubas, *Inorg. Chem.* **2005**, *44*, 8306-8316; b) C. Holzhacker, C. M. Standfest-Hauser, M. Puchberger, K. Mereiter, L. F. Veiros, M. J. Calhorda, M. D. Carvalho, L. P. Ferreira, M. Godinho, F. Hartl, K. Kirchner, *Organometallics* **2011**, *30*, 6587-6601; c) D. Benito-Garagorri, L. G. Alves, L. F. Veiros, C. M. Standfest-Hauser, S. Tanaka, K. Mereiter, K. Kirchner, *Organometallics* **2010**, *29*, 4932-4942.

[9] A. W. Addison, T. N. Rao, J. Reedijk, J. van Rijn, G. C. Verschoor, *J. Chem. Soc., Dalton Trans.* **1984**, 1349-1356.

[10] a) D. R. Burfield, K.-H. Lee, R. H. Smithers, *The Journal of Organic Chemistry* **1977**, *42*, 3060-3065; b) D. R. Burfield, R. H. Smithers, *J. Org. Chem.* **1978**, *43*, 3966-3968; c) D. B. G. Williams, M. Lawton, *The Journal of Organic Chemistry* **2010**, *75*, 8351-8354.

[11] H. Hou, P. K. Gantzel, C. P. Kubiak, *Organometallics* **2003**, *22*, 2817-2819.

[12] a) G. A. Craig, O. Roubeau, G. Aromí, *Coord. Chem. Rev.* **2014**, *269*, 13-31; b) J. A. Kitchen, S. Brooker, *Coord. Chem. Rev.* **2008**, *252*, 2072-2092.

[13] R. Ziessel, V. Grosshenny, M. Hissler, C. Stroh, *Inorg. Chem.* **2004**, *43*, 4262-4271.

[14] E. D. Bloch, M. R. Hudson, J. A. Mason, S. Chavan, V. Crocellà, J. D. Howe, K. Lee, A. L. Dzubak, W. L. Queen, J. M. Zadrozny, S. J. Geier, L.-C. Lin, L. Gagliardi, B. Smit, J. B. Neaton, S. Bordiga, C. M. Brown, J. R. Long, *J. Am. Chem. Soc.* **2014**, *136*, 10752-10761.

[15] A. K. Hui, B. J. Cook, D. J. Mindiola, K. G. Caulton, *Inorg. Chem.* **2014**, *53*, 3307-3310.

[16] D. Zabel, A. Schubert, G. Wolmershäuser, R. L. Jones, W. R. Thiel, *Eur. J. Inorg. Chem.* **2008**, *2008*, 3648-3654.

Author Manuscript

This article is protected by copyright. All rights reserved

Entry for the Table of Contents (Please choose one layout)

Layout 1:

FULL PAPER

Text for Table of Contents

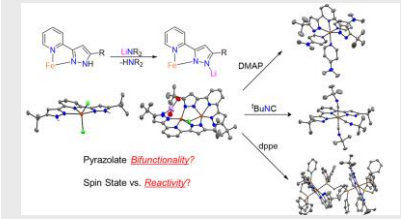

Key Topic*

*Author(s), Corresponding Author(s)**

Page No. – Page No.

Title

Iron Complexes

The process of removal of protons and of chloride, dehydrohalogenation, from $(H_2L)FeCl_2$ is investigated systematically, to understand the reactivity of the implied transient LFe^{II}. The collective evidence from these studies shows that divalent iron is not strongly obedient to the 18 electron rule, although Fe^{II} is faithful to preferred coordination number 6; among all species reported here, only the Fe_2 and Fe_3 species have coordination number 5

Layout 2:

FULL PAPER

((Insert TOC Graphic here; max. width: 11.5 cm; max. height: 2.5 cm; NOTE: the final letter height should not be less than 2 mm.))

Key Topic*

*Author(s), Corresponding Author(s)**

Page No. – Page No.

Title

Text for Table of Contents

*one or two words that highlight the emphasis of the paper or the field of the study

Author Manuscript

This article is protected by copyright. All rights reserved

Author Manuscript

This article is protected by copyright. All rights reserved